

# Long-range donor-acceptor electron transport mediated by $\alpha$ -helices

L.S. Brizhik\*,

Bogolyubov Institute for Theoretical Physics  
of the National Academy of Sciences of Ukraine,  
03143 Kyiv, Ukraine

J. Luo<sup>†</sup>

School of Mathematics, University of Birmingham,  
Birmingham B15 2TT, UK

B.M.A.G. Piette<sup>‡</sup> and W.J. Zakrzewski<sup>§</sup>

Department of Mathematical Sciences, University of Durham,  
Durham DH1 3LE, UK

## Abstract

We study the long-range electron and energy transfer mediated by a polaron on an  $\alpha$ -helix polypeptide chain coupled to donor and acceptor molecules at opposite ends of the chain. We show that for specific parameters of the system, an electron initially located on the donor can tunnel onto the  $\alpha$ -helix, forming a polaron, which then travels to the other extremity of the polypeptide chain where it is captured by the acceptor. We consider three families of couplings between the donor, acceptor and the chain, and show that one of them can lead to a 90% efficiency of the electron transport from donor to acceptor. We also show that this process remains stable at physiological temperatures in the presence of thermal fluctuations in the system.

PACS numbers: 05.45.Yv, 05.60.-k, 63.20.kd, 71.38.-k

---

\*e-mail address: brizhik@bitp.kiev.ua

<sup>†</sup>e-mail address: j.luo.5@bham.ac.uk

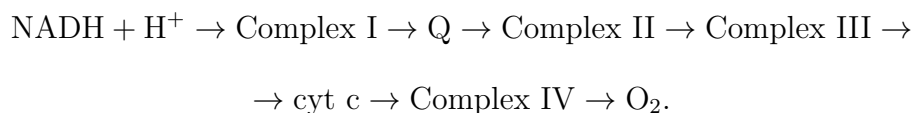
<sup>‡</sup>e-mail address: B.M.A.G.Piette@durham.ac.uk

<sup>§</sup>e-mail address: w.j.zakrzewski@durham.ac.uk

Key words: long-range donor-acceptor electron and energy transfer, large polaron, alpha-helix, donor-bridge-acceptor complex, soliton, self-trapping

## 1 Introduction

The mechanisms behind the highly efficient long-range electron transfer (ET) in redox reactions accompanying photosynthesis and cellular respiration have been intensively discussed over several decades [1, 2]. This transfer takes place at macroscopic distances along the so-called electron transport chain in Krebs cycles in membranes of chloroplasts, mitochondria or cells, and occurs at physiological temperatures. Conventional mechanisms, such as tunnelling, Forster and Dexter mechanism etc. [3, 4, 5], cannot provide such long-range ET even at zero temperature, let alone 300 K. Nevertheless, it should be noted that the very structure of the ET chain can facilitate these processes. An ET chain consists of a spatially separated sequence of biological molecular complexes (peptides, enzymes, etc.), along which the sequential transport of electrons takes place via redox processes, so that every site in this chain plays the role of an acceptor for the left neighbour and donor for the right one along the chain (see, e.g., [6]). The electron transport chain in mitochondria can be schematically represented as the following sequence:



Here  $\text{NADH} + \text{H}^+$  is nicotinamide adenine dinucleotide, which serves as the substrate; Complex I is NADH coenzyme Q reductase; Q is ubiquinone coenzyme; Complex II is succinate dehydrogenase; Complex III is cytochrome  $\text{bc}_1$ ; cyt  $c$  is cytochrome  $c$ ; Complex IV is cytochrome  $c$  oxidase;  $\text{O}_2$  is molecular oxygen. Another example of the electron transport chain can be found in [7].

In each elementary process, at the onset, there is a release of four electrons at the substrate, which then are carried along the chain with the reduction of molecular oxygen and hydrogen ions to a water molecule at the final stage of the process. This transport of electrons is so exceptionally efficient that only a tiny percentage of electrons leak out to reduce oxygen. The complexes in the ET chain can be conventionally divided into two groups: heavy and light ones. In particular, in ET chains, such elements as ubiquinone or cytochrome  $\text{cyt-}c$ , have relatively small molecular weight which leads to their high mobility. They can move outside the mitochondrial membrane, carrying

electrons from a heavy donor to a heavy acceptor via a linear, *e.g.* the Forster mechanism [3, 5]. Some other complexes in the electron transport chain, such as NADH-ubiquinone oxireductase, flavoproteids, cytochrome *c*-oxidase, cyt *aa*<sub>3</sub> and cytochrome cyt *bc*<sub>1</sub> are proteins with large molecular weight of up to several hundreds of kiloDaltons. Conventional linear mechanisms cannot provide coherent transport of electrons across these heavy enzymes, either as a whole or internally between co-factors separated by macroscopic distances, for instance porphyrins, metal clusters etc., that are separated by macroscopic distance. Nevertheless, their regular crystal-like structure can facilitate ET, as is discussed below. For instance, inside some large enzymes like NADH ubiquinone oxidoreductase there can be several long pathways for electron transport [2], where one can identify the alpha-helical part of the enzyme between the donor and the acceptor.

A significant part of heavy macromolecules is in the alpha-helical conformation, whose regular structure results in the formation of electron bands in their energy spectrum. The alpha-helical structure is stabilized by relatively weak hydrogen bonds resulting in strong electron-lattice interactions, and thus, in the polaron effect. An  $\alpha$ -helical segment of a protein contains three almost-parallel polypeptide strands bound by hydrogen bonds along the strands, with weak interactions between these strands. An isolated strand is described by the Fröhlich Hamiltonian, and this description leads to a system of coupled nonlinear equations for the electron wavefunction and lattice variables, and admits soliton solutions. The possibility of self-trapping of electrons in an isolated one-dimensional molecular chain, like a polypeptide strand, has been first shown in [8] (see also [9, 10]) and later it was also demonstrated in helical systems [11, 12, 13]. The soliton solutions of these models are particular cases of a large polaron. Such a polaron can be described as a crossover between an almost-free electron and small polaron states depending on the strength of the exchange interaction energy, electron-lattice coupling constant, the number of phonon modes, their type and the corresponding Debye energies [14]. The soliton properties depend on the parameters of the system. Moreover, the helical structure of proteins was shown to lead to the existence of several types of soliton solutions of the model with different properties and symmetries [13]. In such soliton states electrons can propagate along macromolecules almost without any loss of energy.

The results mentioned above have been obtained for isolated strands or helices, while in reality, the electron transport occurs in the system Donor-Bridge-Acceptor, as is the case for the ET chain in the Krebs cycles. The simple case when the bridge is modelled as a polypeptide strand had been studied in [15]. It was shown there that the long-range ET can be provided

by the soliton mechanism within a wide range of parameter values of donor, acceptor and polypeptide strands.

In the present paper we study the possibility of a coherent long-range electron transport in the system Donor- $\alpha$ -helix-acceptor. As one can expect, the formation of the soliton on the  $\alpha$ -helix depends on the helix-donor and helix acceptor coupling, as well as on the parameters of the system under study (see *e.g.*, [15, 16, 17]), and we can find conditions which lead to the formation of a soliton on the helix.

There are two other aspects of the model developed in the present paper. The first one is related to the fact that the functioning of the ET chain is tightly connected with the production of adenosine triphosphate (ATP): in most organisms the majority of ATP is generated in ET chains (see, *e.g.*, [18]). The energy of the hydrolysis of ATP into ADP is the basic unit of energy used in biological systems, in particular, in muscles to produce mechanical work, to establish electrochemical gradients across membranes, in biosynthetic processes, and in many other physiological and biochemical processes necessary to maintain life. The amount of energy released by ATP hydrolysis is approximately 0.43 eV, which is only 20 times the thermal energy at physiological temperatures and is not enough for an electronic excitation. It is sufficient to excite some vibrations, such as an AMID I vibration, an excitation which requires an energy of 0.21 eV. AMID I is mainly (up to 80%) the stretching vibration of double C=O bond of the peptide group which has a relatively large dipole moment 0.3 Db oriented along the alpha-helix axis. This excitation is registered in optical spectra of polypeptide molecules, its wavelength being  $1650\text{ cm}^{-1}$ , and, according to [19], the ATP hydrolysis energy is transferred along protein macromolecules in the form of AMID I vibration. For more details see [20, 21, 9, 10, 22] or more recently [23, 24].

As has been shown by Davydov, the Amide-I vibration can be self-trapped in macromolecule into a soliton state and carried along it to the place where it is utilized for biochemical or mechanical needs [9, 10]. This process, from the mathematical point of view, is described formally by the same system of equations as the ET. Therefore, the results obtained here are equally valid for such energy transfer processes.

The second aspect of the model is related to the potential importance of our results for micro- and nano-electronics where conjugated donor-acceptor copolymer semiconductors with intra-molecular charge transfer on large distances are widely used. A large number of such systems have been recently synthesized. They include donor-acceptor pairs mediated by salt bridges [25], thienopyrazine-based copolymers [26] and some others [27, 28, 29]. Donor-bridge-acceptor systems with efficient ET play an important role in electronic applications [30, 31, 32, 33]: they can be used in photovoltaic cells

[34, 35, 36, 29], light-emitting diodes [37, 38, 39, 40] and field-effect transistors [41, 42, 43, 44], in particular, thin-film organic field effect transistors [45]. Proteins and synthetic macromolecules have a great technological potential; one example is the improvement of efficiency and UV-photostability of planar perovskite solar cells using amino-functionalized conjugated polymers as ET materials [27, 29].

Recent novel applications in bioelectronics such as organic photovoltaics, fuel cell technology and other, are based on metalorganic frameworks or structures, that are complexes of electroconducting compounds/substrates and polypeptides (see, e.g., [46, 47, 48] and references therein). It has been shown that both the peptide composition and structure can affect the efficiency of electron transport across peptides [47]. Moreover, long-range conductivity and enhanced solid-state electron transport in proteins and peptide bioelectronic materials has been proven experimentally [49, 50]. The effectiveness of electron transport processes in living systems is already used in novel electronic devices, e.g., in *Shewanella Oneidensis* MR-1 Cells, based on multiheme cytochrome mediated redox conduction [51], or in synthesized supramolecular charge transfer nanostructures based on peptides [52], synthetic biological protein nanowires with high conductivity [53], self-assembled peptide nanotubes used as electronic aterials [54] and many others. We quote [49]: The ability of such natural and synthetic protein and peptide materials to conduct electricity over micrometer to centimeter length scales, however, is not readily understood from a conventional view of their amino acid building blocks. Distinct in structure and properties from solid-state inorganic and synthetic organic metals and semiconductors, supramolecular conductive proteins and peptides require careful theoretical treatment. This is one of the factors which have motivated our interest in the problems discussed in the present paper and we hope that our study will shed some light on this problem.

In the first section of the paper we derive a model of the  $\alpha$ -helix coupled to a donor molecule and an acceptor molecule. This model is a combination of the models derived in [13] and [15]. We then perform a parameter scaling to make all the parameters dimensionless and derive the equations in such units. After selecting the parameters that best describe the  $\alpha$ -helical protein, we compute the profile of a static self-trapped electron state (soliton-like or, in other words, large polaron state, which for simplicity we call from now on a ‘polaron’) by solving the model equations numerically. We then study various configurations where the electron density has been set to 1 on the donor and 0 elsewhere and let the system evolve. We do this for three different types of couplings between the donor and acceptor to the  $\alpha$ -helix and we determine numerically the donor and acceptor coupling parameters that lead to the best

transfers of the electron. We end the paper by describing the solutions we have found and draw some conclusions.

## 2 Model of the System ‘Donor – $\alpha$ -Helix – Acceptor’

We consider a polypeptide chain in an  $\alpha$ -helical configuration made out of  $N$  peptide groups (PGs), with a donor molecule attached to one end and an acceptor molecule attached to the other end. The peptide chain forms a helical structure in which each molecule is coupled by chemical bonds to its neighbours along the chain as well as to the PG 3 sites away from it by hydrogen bonds. With this 3-step coupling, the  $\alpha$ -helix can also be seen as 3 parallel chains [55] which we refer to as strands in what follows. This model is depicted in Fig. 1.

We label the PGs with the index  $n$  along the polypeptide chain, and use  $n = 0$  for the donor and  $n = N + 1$  for the acceptor. This means that PGs with an index difference which is a multiple of 3 belong to the same strand of the  $\alpha$ -helix.

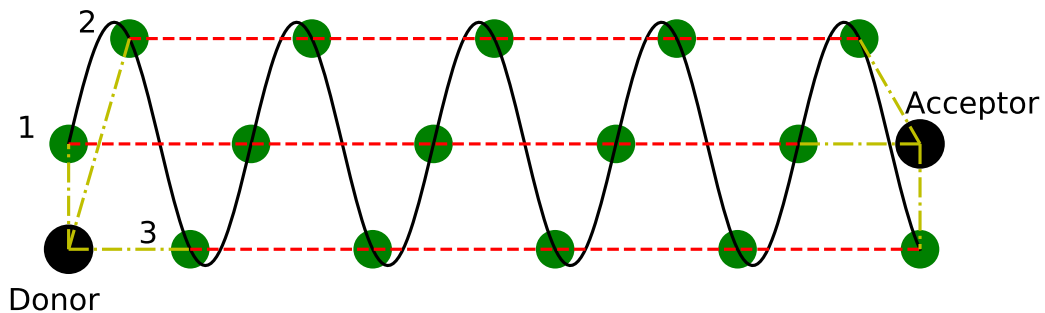


Figure 1: The model of  $\alpha$ -helix with a donor and an acceptor. The continuous line represents the helix backbone formed by chemical bonds, the dash lines represent the hydrogen bonds that are links along the strands and the dash-dot lines the links between the donor/acceptor and the different strands. The numbers 1, 2 and 3 label the 3 strands.

The donor and the acceptor can, *a-priori*, be coupled respectively to the first 3 and the last 3 peptides, *i.e.*, with the nodes  $n = 1, 2, 3$  and  $N =$

$N - 2, N - 1, N$ . In our study, we will consider 3 different types of couplings but for now, we assume that all the coupling parameters are different.

The Hamiltonian of the system is given by

$$\mathcal{H} = \mathcal{H}_e + \mathcal{H}_p + \mathcal{H}_{int}, \quad (1)$$

where  $\mathcal{H}_e$ ,  $\mathcal{H}_p$  and  $\mathcal{H}_{int}$  are respectively the phonon, electron and interaction Hamiltonians given by

$$\begin{aligned} \mathcal{H}_e = & \bar{E}_d |\Psi_0|^2 + \bar{E}_a |\Psi_{N+1}|^2 + \bar{E}_0 \sum_{n=1}^N |\Psi_n|^2 - \bar{J} \sum_{n=1}^{N-3} \left( \Psi_n \Psi_{n+3}^* + \Psi_{n+3} \Psi_n^* \right) \\ & + \bar{L} \sum_{n=1}^{N-1} \left( \Psi_n \Psi_{n+1}^* + \Psi_{n+1} \Psi_n^* \right) - \sum_{\ell=1}^3 \bar{D}_{d,\ell} (\Psi_0 \Psi_\ell^* + \Psi_\ell \Psi_0^*) \\ & - \sum_{\ell=1}^3 \bar{D}_{a,\ell} (\Psi_{N+1} \Psi_{N-3+\ell}^* + \Psi_{N-3+\ell} \Psi_{N+1}^*), \end{aligned} \quad (2)$$

$$\begin{aligned} \mathcal{H}_p = & \frac{1}{2} \left[ \frac{P_d^2}{M_d} + \frac{P_a^2}{M_a} \right] + \frac{1}{2} \sum_{\ell=1}^3 \left[ \bar{W}_{d,\ell} (U_0 - U_\ell)^2 + \bar{W}_{a,\ell} (U_{N+1} - U_{N-3+\ell})^2 \right] \\ & + \frac{1}{2} \sum_{n=1}^N \frac{P_n^2}{M} + \frac{1}{2} \sum_{n=1}^{N-3} \bar{W} (U_{n+3} - U_n)^2, \end{aligned} \quad (3)$$

$$\begin{aligned} \mathcal{H}_{int} = & |\Psi_0|^2 \sum_{\ell=1}^3 \bar{\chi}_{d,\ell} (U_\ell - U_0) + |\Psi_{N+1}|^2 \sum_{\ell=1}^3 \bar{\chi}_{a,\ell} (U_{N+1} - U_{N-3+\ell}) \\ & + \sum_{\ell=1}^3 |\Psi_\ell|^2 \left[ \bar{\chi}_{d,\ell} (U_\ell - U_0) + \bar{\chi} (U_{\ell+3} - U_\ell) \right] \\ & + \sum_{\ell=1}^3 |\Psi_{N-3+\ell}|^2 \left[ \bar{\chi}_{a,\ell} (U_{N+1} - U_{N-3+\ell}) + \bar{\chi} (U_{N-3+\ell} - U_{N-6+\ell}) \right] \\ & + \bar{\chi} \sum_{n=4}^{N-3} |\Psi_n|^2 (U_{n+3} - U_{n-3}). \end{aligned} \quad (4)$$

In these expressions,  $\bar{E}_0$  describes the on-site electron energy,  $\bar{J}$  the resonance integral along the strands,  $\bar{L}$  the resonance integral along the helix,  $M$  the mass of the unit cell,  $\bar{\chi}$  the electron-lattice coupling and  $\bar{W}$  the elasticity of the bond along the strands. The constants with subscript  $d$  and  $a$  refer to parameters of the donor and the acceptor respectively.

The functions  $\Psi_n$  describe the electron wave function (and so  $|\Psi_n|^2$  describe the electron probability of being at the site  $n$ ) and  $U_n$  describe the

displacement of molecule  $n$  along the strands.  $P_n$  are the canonically conjugated momenta of  $U_n$ . Of course, the electron wave function satisfies the normalization condition

$$\sum_{n=0}^{N+1} |\Psi_n|^2 = 1, \quad (5)$$

where, following our convention,  $\Psi_0 = \Psi_d$  and  $\Psi_{N+1} = \Psi_a$ .

Our model is meant to describe the case in which the principal chain can be sufficiently well approximated by one phonon band corresponding to an acoustical phonon mode which describes the longitudinal displacements of the unit cells from their positions of equilibrium along the helix's strands. The electron-lattice interaction Hamiltonian induces a dependence of the electron Hamiltonian on the lattice distortions. We also assume here that the dependence of the on-site electron energy on the lattice distortion is much stronger than that of the inter-site electron interaction energy.

The model we present here is a combination of the polaron model of the  $\alpha$ -helix which was described in detail in [13] and of the donor-acceptor model described in [15]. The first model describes polarons on an  $\alpha$ -helix, instead of using the traditional single chain, proposed by Davydov [9, 10], which corresponds to what we call a strand in this paper. In fact, it was shown in [13] that the polaron is spread over the 3 strands hence the relevance of using a more realistic helical model. The second paper describes a model of the transfer of an electron from a donor molecule to an acceptor one via the coherent propagation of a polaron along a simple chain (a single strand in the present model). The model we describe here is a combination of these two models in which the donor and the acceptor are coupled to a proper  $\alpha$ -helix instead of to a single strand.

### 3 Parameter scaling

To facilitate the analysis of the model solutions, it is convenient to scale the parameters so that they become dimensionless. Thus, following [13], we perform the following scalings:

$$\begin{aligned} d &= 10^{-11} \text{ m}, & u_n &= \frac{U_n}{d}, & \tau &= t\nu, \\ E_0 &= \frac{\bar{E}_0}{\hbar\nu}, & E_d &= \frac{\bar{E}_d}{\hbar\nu}, & E_a &= \frac{\bar{E}_a}{\hbar\nu}, \\ J &= \frac{\bar{J}}{\hbar\nu}, & D_a &= \frac{\bar{D}_a}{\hbar\nu}, & D_d &= \frac{\bar{D}_d}{\hbar\nu}, \\ W &= \frac{\bar{W}}{\nu^2 M}, & W_{d,\ell} &= \frac{\bar{W}_{d,\ell}}{\nu^2 M}, & W_{a,\ell} &= \frac{\bar{W}_{a,\ell}}{\nu^2 M}, \\ \chi &= \frac{d\bar{\chi}}{\hbar\nu}, & \chi_{d,\ell} &= \frac{d\bar{\chi}_{d,\ell}}{\hbar\nu}, & \chi_{a,\ell} &= \frac{d\bar{\chi}_{a,\ell}}{\hbar\nu}, \\ L &= \frac{\bar{L}}{\hbar\nu}, & K_d &= \frac{\bar{M}}{M_d}, & K_a &= \frac{\bar{M}}{M_a}. \end{aligned} \quad (6)$$



As a result, the Hamiltonian takes the form  $\mathcal{H}_p = M \nu^2 d^2 H_p$ ,  $\mathcal{H}_e = \hbar \nu H_e$  and  $\mathcal{H}_{int} = \hbar \nu H_{int}$  where the dimensionless terms are

$$\begin{aligned}
H_e = & E_d |\Psi_0|^2 + E_a |\Psi_{N+1}|^2 + E_0 \sum_{n=1}^N |\Psi_n|^2 - J \sum_{n=1}^{N-3} \left( \Psi_n \Psi_{n+3}^* + \Psi_{n+3} \Psi_n^* \right) \\
& + L \sum_{n=1}^{N-1} \left( \Psi_n \Psi_{n+1}^* + \Psi_{n+1} \Psi_n^* \right) - \sum_{\ell=1}^3 D_{d,\ell} (\Psi_0 \Psi_\ell^* + \Psi_\ell \Psi_0^*) \\
& - \sum_{\ell=1}^3 D_{a,\ell} (\Psi_{N+1} \Psi_{N-3+\ell}^* + \Psi_{N-3+\ell} \Psi_{N+1}^*), \tag{7}
\end{aligned}$$

$$\begin{aligned}
H_p = & \frac{1}{2} \left[ \frac{1}{K_d} \left( \frac{du_0}{dt} \right)^2 + \frac{1}{K_a} \left( \frac{du_{N+1}}{dt} \right)^2 \right] + \\
& + \frac{1}{2} \sum_{\ell=1}^3 \left[ W_{d,\ell} (u_0 - u_\ell)^2 + W_{a,\ell} (u_{N+1} - u_{N-3+\ell})^2 \right] \\
& + \frac{1}{2} \sum_{n=1}^N \left( \frac{du_n}{dt} \right)^2 + \frac{1}{2} \sum_{n=1}^{N-3} W (u_{n+3} - u_n)^2, \tag{8}
\end{aligned}$$

$$\begin{aligned}
H_{int} = & |\Psi_0|^2 \sum_{\ell=1}^3 \chi_{d,\ell} (U_\ell - U_0) + |\Psi_{N+1}|^2 \sum_{\ell=1}^3 \chi_{a,\ell} (U_{N+1} - U_{N-3+\ell}) \\
& + \sum_{\ell=1}^3 |\Psi_\ell|^2 [\chi_{d,\ell} (U_\ell - U_0) + \chi (U_{\ell+3} - U_\ell)] \\
& + \sum_{\ell=1}^3 |\Psi_{N-3+\ell}|^2 [\chi_{a,\ell} (U_{N+1} - U_{N-3+\ell}) + \chi (U_{N-3+\ell} - U_{N-6+\ell})] \\
& + \chi \sum_{n=4}^{N-3} |\Psi_n|^2 (U_{n+3} - U_{n-3}). \tag{9}
\end{aligned}$$

We must thus have  $M \nu^2 d^2 = \hbar \nu$  and so  $\nu = \hbar / (M d^2)$ . With  $M = 1.9112 \times 10^{-25}$  kg [15] and, as  $\hbar = 1.054 \times 10^{-34}$  Js, we have  $\nu = 5.51 \times 10^{12}$  s<sup>-1</sup>.

Before deriving the dimensionless equations it is also convenient to multiply the wave function by a time-dependent phase and so we define

$$\psi(t) = \Psi(t) \exp \left( -\frac{it}{\hbar} (\bar{E}_0 + 2\bar{L} - 2\bar{J}) \right). \tag{10}$$

Following [15] we also add to the acceptor equation a term of the form  $i \sum_{\ell=1}^3 A_{a,\ell} |\psi_{N-3+\ell}|^2 \psi_{N+1}$ , which describes the transfer of the electron from

the alpha-helix to the acceptor and has a clear physical meaning: the higher the probability of the electron localization at the terminal end of the helix, the higher the probability of its transfer to the acceptor. It is easy to check that this extra term does not violate conservation of the total electron probability.

From the above Hamiltonian (1),(7)-(9) one can easily derive the following equations for  $U_n$  and  $\Psi_n$ :

$$\begin{aligned}
i\frac{d\Psi_0}{d\tau} &= (E_d - E_0 - 2L + 2J)\Psi_0 - \sum_{\ell=1}^3 D_{d,\ell}\Psi_\ell + \Psi_0 \sum_{\ell=1}^3 \chi_{d,\ell}(u_\ell - u_0), \\
i\frac{d\Psi_\ell}{d\tau} &= (2J - 2L)\Psi_\ell - J\Psi_{\ell+3} + L(\Psi_{\ell+1} + \Psi_{\ell-1}(1 - \delta_{\ell,1})) - D_{d,\ell}\Psi_0 \\
&\quad + \chi_{d,\ell}\Psi_\ell(u_\ell - u_0) + \chi\Psi_\ell(u_{\ell+3} - u_\ell), \quad \ell = 1, 2, 3, \\
i\frac{d\Psi_n}{d\tau} &= (2J - 2L)\Psi_n - J(\Psi_{n+3} + \Psi_{n-3}) + L(\Psi_{n+1} + \Psi_{n-1}) + \chi\Psi_n(u_{n+3} - u_{n-3}), \\
&\quad n = 4 \dots N - 3, \\
i\frac{d\Psi_{N-3+\ell}}{d\tau} &= (2J - 2L)\Psi_{N-3+\ell} - J\Psi_{N-6+\ell} + L(\Psi_{N-4+\ell} + \Psi_{N-2+\ell}(1 - \delta_{\ell,3})) - D_{a,\ell}\Psi_{N+1} \\
&\quad + \chi_{a,\ell}\Psi_{N-3+\ell}(u_{N+1} - u_{N-3+\ell}) + \chi\Psi_{N-3+\ell}(u_{N-3+\ell} - u_{N-6+\ell}) \\
&\quad - iA_{a,\ell}|\Psi_{N+1}|^2\Psi_{N-3+\ell}, \quad \ell = 1, 2, 3, \\
i\frac{d\Psi_{N+1}}{d\tau} &= (E_a - E_0 + 2J - 2L)\Psi_{N+1} - \sum_{\ell=1}^3 D_{a,\ell}\Psi_{N-3+\ell} + \Psi_{N+1} \sum_{\ell=1}^3 \chi_{a,\ell}(u_{N+1} - u_{N-3+\ell}) \\
&\quad + i\sum_{\ell=1}^3 A_{a,\ell}|\Psi_{N-3+\ell}|^2\Psi_{N+1}, \\
\frac{d^2u_0}{d\tau^2} &= K_d\left(\sum_{\ell=1}^3 W_{d,\ell}(u_\ell - u_0) + \sum_{\ell=1}^3 \chi_{d,\ell}(|\Psi_0|^2 + |\Psi_\ell|^2)\right), \\
\frac{d^2u_\ell}{d\tau^2} &= W(u_{\ell+3} - u_\ell) + W_{d,\ell}(u_0 - u_\ell) - \chi_{d,\ell}(|\Psi_0|^2 + |\Psi_\ell|^2) + \chi(|\Psi_\ell|^2 + |\Psi_{\ell+3}|^2), \\
&\quad \ell = 1, 2, 3, \\
\frac{d^2u_n}{d\tau^2} &= W(u_{n+3} + u_{n-3} - 2u_n) + \chi(|\Psi_{n+3}|^2 - |\Psi_{n-3}|^2), \quad n = 4 \dots N - 3, \\
\frac{d^2u_{N-3+\ell}}{d\tau^2} &= W(u_{N-6+\ell} - u_{N-3+\ell}) + W_{a,\ell}(u_{N+1} - u_{N-3+\ell}) \\
&\quad + \chi_{a,\ell}(|\Psi_{N+1}|^2 + |\Psi_{N-3+\ell}|^2) - \chi(|\Psi_{N-3+\ell}|^2 + |\Psi_{N-6+\ell}|^2), \quad \ell = 1, 2, 3, \\
\frac{d^2u_{N+1}}{d\tau^2} &= K_a\left(\sum_{\ell=1}^3 W_{a,\ell}(u_{N-3+\ell} - u_{N+1}) - \sum_{\ell=1}^3 \chi_{a,\ell}(|\Psi_{N+1}|^2 + |\Psi_{N-3+\ell}|^2)\right), \quad (11)
\end{aligned}$$

where  $\delta_{i,j}$  is the Kronecker delta function. We now need to select the param-

eter values that best describe the  $\alpha$ -helix.

### 3.1 Parameter values

For the numerical modelling we need to use some numerical values of the parameters. We recall that, in particular, the parameter values for the polypeptide macromolecules are:  $J_{\text{Amide-I}} = 1.55 \times 10^{-22}$  Joules  $\approx 10^{-3}$  eV;  $J_e \approx 0.1 - 0.01$  eV  $\approx 10^{-21} - 10^{-20}$  Joules;  $\chi = (35 - 62)$  pN;  $w = 39 - 58$  N/m,  $V_{ac} = (3.6 - 4.5) \times 10^3$  m/s [10]. The molecular weights of large macromolecules which participate in the electron transport chain in redox processes are: NADH-ubiquinone oxidoreductase - 980 kDa; cytochrome  $bc_1$  complex - 480 kDa; cytochrome  $c - aa_3$  oxidase - 420 kDa. The mass of Cyt-c is 12 kDa, in which the hem-A group has a molecular weight 852 Da, and hem-B group has 616 Da, which are 3-5 times larger than the molecular weight, 100-200 Da, of amino-acids that form macromolecules. Studies of the mitochondrial ET chain shows that the electrochemical potential for the transfer of an electron is  $E_{e-c} = +1.135$  V [56, 57].

For completeness of the study we also summarize the data on the parameter values of other relevant compounds in accordance with the discussion in the introduction. The molecular weights of many conjugated polymer semiconductors vary in the interval (10 - 176) kDa, and the hole mobility is  $4 \times 10^{-4} - 1.6 \times 10^{-3}$  cm<sup>2</sup>/(V s). The ionization potential and electron affinity potential for some donor-acceptor copolymer semiconductor molecules are: (2.5-4.5) eV and (1.5-3.1) eV, respectively [58]. The electrochemical band gap is  $E_g^{(el)} = E_{IP} - E_{EA}$  is 1.5 eV for BTTP, 1.84 eV for BTTP-P, and 2.24 eV for BTTP-F, which are 0.4-0.6 eV larger from the optically determined ones  $E_g^{(opt)} = 1.1 - 1.6$  eV. This difference can be explained by the exciton binding energy of conjugated polymers which is thought to be in the range of  $E_{ex} \approx 0.4 - 1.0$  eV [59]. Thieno pyrazine-based donor-acceptor copolymers, such as BTTP, BTTP-T, BTTP-F, BTTP-P, have moderate to high molecular weights, broad optical absorption bands that extend into the near-infrared region with absorption maxima at 667-810 nm, and small optical band gaps (1.1 - 1.6 eV). They show ambipolar redox properties with low ionization potentials (HOMO levels) of (4.6-5.04) eV. The field-effect mobility of holes varies from  $4.2 \times 10^{-4}$  cm<sup>2</sup>/(V s) in BTTP-T to  $1.6 \times 10^{-3}$  cm<sup>2</sup>/(V s) in BTTP-F (see [26]). The reduction potentials of BTTP, BTTP-P, and BTTP-F are -1.4, -1.73, and -1.9 V (vs SCE), respectively. The oxidation potentials of the copolymers are in the range 0.29-0.71 V (vs SCE). The onset oxidation potential and onset reduction potential of the parent copolymer BTTP are 0.2 and -1.3 V, respectively, which give an estimate for the ionization potential (IP, HOMO level) of 4.6 eV ( $E_{IP} = E_{ox}^{onset} + 4.4$ ) and an

electron affinity (EA, LUMO level) of 3.1 eV ( $E_{EA} = E_{red}^{onset} + 4.4$ ). The 4.6 eV  $E_{IP}$  value of BTTP is 0.3 eV lower than that of poly(3-hexylthiophene) (4.9 eV), whereas its  $E_{EA}$  value (3.1 eV) is 0.6 eV higher than that reported for the poly(2,3-dioctylthieno[3,4-b]pyrazine) homo-polymer ( $\approx 2.5$  eV). An  $E_{IP}$  value of 4.64 eV and  $EEA$  value of 2.8 eV were found in the case of BTTP-P [26].

In what follows, we set the on-site electron energy level as the zero of energy, hence we take  $\bar{E}_0 = 0$ . We are also using a set of model parameters close to those encountered in polypeptide macromolecules or to the bridge-mediated donor-acceptor systems summarized above *i.e.*

$$\bar{J} = 8.42 \times 10^{-23} \text{ J}, \quad \bar{L} = 1.34 \times 10^{-22} \text{ J}, \quad \bar{W} = 10.59 \text{ kg/s}^2, \quad \bar{\chi} = 1.85 \times 10^{-11} \text{ J/m} \quad (12)$$

corresponding to the following adimensional values of the parameters in our equations

$$J = 0.145, \quad L = 0.231, \quad W = 1.825, \quad \chi = 0.318. \quad (13)$$

The order of magnitude of these parameters values is close to the parameter values for the electron transport in polypeptides and for other systems described above. Our aim, for these systems, is to establish a proof of concept of the soliton mediated long-range ET rather than a performing a detailed study of their actual fine properties.

Before studying the transfer of an electron from the donor to the acceptor we have computed the profile of the static polaron on the helix for the parameters given in (13). This profile is shown on Fig. 2. To obtain this profile, we have relaxed the equations (11), using donor-acceptor parameter values so that they do not interact with the chain.

One sees clearly from Fig. 2, where the index  $i$  runs along the polypeptide helix and where each curve corresponds to a different strand, that the static polaron is a broad localised lump which winds around the polypeptide chain rather than a single soliton located on a single strand or three identical solitons located on each of the strands.

## 4 Classes of Couplings

Having so far defined a model with a general set of couplings between the  $\alpha$ -helix and the donor and acceptor, we will now restrict ourselves to 3 families of couplings.

In the first set, the donor and the acceptor are coupled to all 3 strands of the helix using identical coupling parameters. So we have

$$D_{d,1} = D_{d,2} = D_{d,3} \neq 0, \quad D_{a,1} = D_{a,2} = D_{a,3} \neq 0,$$

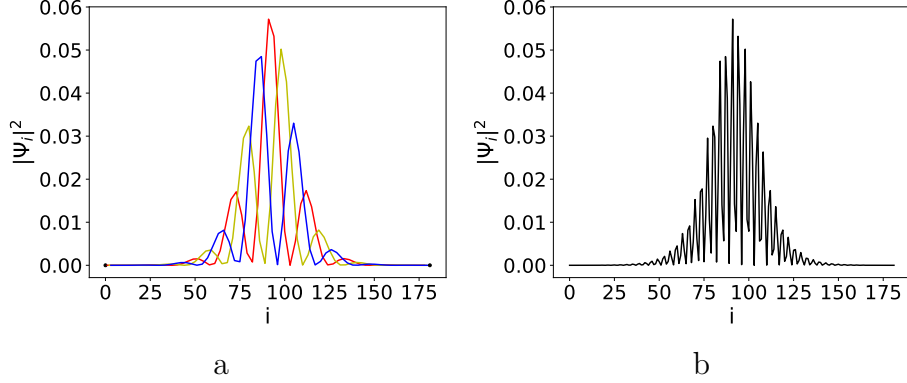


Figure 2: Polaron with  $E_0 = E_d = E_a = 0$ ,  $J = 0.145$ ,  $L = D_{d,3} = D_{a,1} = 0.231$ ,  $D_{d,1} = D_{d,2} = D_{a,2} = D_{a,3} = 0$ ,  $W = W_{d,1} = W_{d,2} = W_{d,3} = W_{a,3} = 1.825$ ,  $W_{a,1} = W_{a,2} = 0$ ,  $\chi_{d,\ell} = 0.318$ ,  $\chi_{d,\ell} = \chi_{a,\ell} = 0$ ,  $A_{a,\ell} = 0$ ,  $K_d = K_a = 1$ . a) The electron probability densities are plotted versus the index on the polypeptide chain. The 3 strands profiles are shown as separate curves. b) The electron density along the  $\alpha$ -helix backbone.

$$W_{d,1} = W_{d,2} = W_{d,3} \neq 0, \quad W_{a,1} = W_{a,2} = W_{a,3} \neq 0. \quad (14)$$

We call such a configuration the ‘full homogeneous’ coupling.

The second configuration describes the case in which the donor and the acceptor are coupled to only one strand, so that

$$\begin{aligned} D_{d,1} \neq 0, \quad D_{d,2} = D_{d,3} = 0, \quad D_{a,1} \neq 0, \quad D_{a,2} = D_{a,3} = 0, \\ W_{d,1} \neq 0, \quad W_{d,2} = W_{d,3} = 0, \quad W_{a,1} \neq 0, \quad W_{a,2} = W_{a,3} = 0, \\ A_{a,1} \neq 0, \quad A_{a,2} = A_{a,3} = 0. \end{aligned} \quad (15)$$

We call this the ‘single strand’ coupling. Notice that the donor is coupled to the first peptide of the helix, *i.e.*, to the first peptide group of the first strand, but the acceptor is coupled to the second but last peptide of the helix, *i.e.*, to the last peptide group on the same strand.

For the third configuration we consider the case when the donor and the acceptor are coupled only to the first and last peptides on the alpha-helix so

$$D_{d,1} \neq 0, \quad D_{a,3} \neq 0, \quad W_{d,1} \neq 0, \quad W_{a,3} \neq 0, \quad A_{a,3} \neq 0, \quad (16)$$

while the other parameters are equal to zero. We call this case the ‘end to end’ coupling.

To find the best parameter values for the transfer of the electron from the donor to the acceptor, we have integrated the system of equations (11)

numerically on a lattice of 180 PGs. As the initial condition we have set the electron probability density to 1 on the donor and to 0 everywhere else. We then integrated the equations (11) numerically up to  $\tau = 500$ . This time was so chosen because it is roughly 3 times longer than it takes for the polaron to reach the end of the 180-peptides chain. The value of  $|\Psi_{N+1}|^2$  varies with time, but tends to increase modulo some oscillations. To evaluate  $\max |\Psi_{N+1}|^2$  we have tracked its value during the evolution and recorded the largest value obtained before  $\tau \leq 500$ .

We have first determined the best donor parameters so that the electron is fully transferred onto the  $\alpha$ -helix. We then scanned a very large range of parameter values for the acceptor to determine the one for which the maximum value of the electron probability density on the acceptor,  $\max |\Psi_{N+1}|^2$ , reaches the largest value.

We will now describe the results we have obtained for each type of coupling.

## 4.1 Full Homogeneous Coupling

The best parameter values we have found to generate a transfer of electron from the donor to the acceptor are (assuming all the values of  $A_{a,\ell}$ ,  $D_{d,\ell}$ ,  $D_{a,\ell}$ ,  $W_{d,\ell}$ ,  $W_{a,\ell}$ ,  $\chi_{d,\ell}$  and  $\chi_{a,\ell}$  are the same for  $\ell = 1, 2, 3$ ):

$$\begin{aligned} E_d &= 0.25, & D_{d,\ell} &= 0.38 J, & W_{d,\ell} &= 0.32 W, & \chi_{d,\ell} &= 0.62 \chi, \\ A_{a,\ell} &= 0.62, & E_a &= 0.194, & D_{a,\ell} &= 0.175 J, & W_{a,\ell} &= 0.14 W, & \chi_{a,\ell} &= 0.27 \chi, \end{aligned} \quad (17)$$

and we have found that  $\max |\Psi|^2 = 0.896$  for  $\tau \leq 500$ .

In Fig. 3 we present the plots of the time evolution of the electron probability density for the parameters values (13) and (17). We see very clearly that the electron is transferred from the donor onto the helix and that it then forms a localized wave that propagates along the helix (see the movie in the supplementary material) and has a complex structure. To understand this result, we have to recall the study of soliton formation in alpha-helices [13] disregarding the donor-acceptor problem. There it has been shown that there exist several types of solitons with different energies and symmetries. This comes from the fact that in the energy spectrum of alpha-helix there are 3 peptide groups per elementary cell and so three electron energy bands which correspond to the Davydov splitting. One of these bands is symmetric and has its minimum in the center of the Brillouin zone, at the wavevector  $k = 0$ , while the other two non-symmetric lower energy bands are degenerate and have their minima at respectively  $k_0 = \pm 9\bar{L}/(\sqrt{3}(18\bar{J} + \bar{L}))$ . As a result, solitons of the first type are formed by the electron from the higher

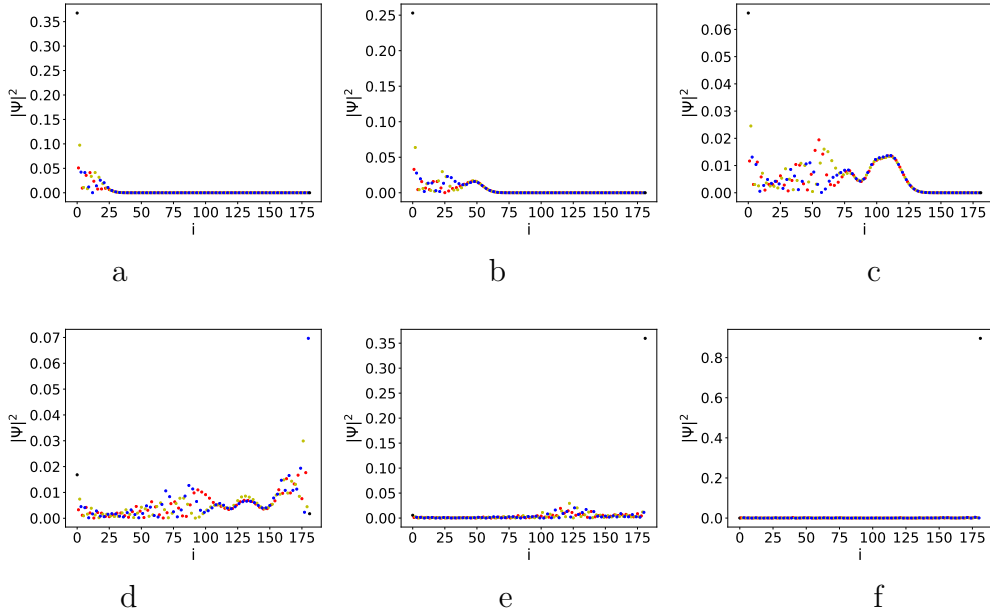


Figure 3: Profile of  $|\Psi|^2$  for the full homogeneous coupling during the transfer from donor to acceptor. a)  $\tau = 25$ , b)  $\tau = 50$ , c)  $\tau = 100$ , d)  $\tau = 150$ , e)  $\tau = 200$ , f)  $\tau = 500$ .

energy band and have an energy, which is split from the higher energy band bottom. On the other hand, the solitons of the second type have energies which are split from the degenerate energy band bottoms and are lower than the energy of the first type of soliton. More importantly, there is an 'hybrid' soliton formed by the entanglement (hybridization) of electron probabilities in the two lowest bands due to the Jan-Teller effect and this soliton has the longest life-time. For the alpha-helix parameter values, which we use in our simulations, this hybrid soliton has an energy which is almost 50 times lower than the energy of the first type of soliton. We can expect, and indeed we will see in what follows, that the full homogeneous coupling provide the best conditions for launching the hybrid soliton in the helix as it has the lowest energy and hence leads to the highest probability for the electron to be transported to the opposite end of the helix.

The complex soliton-like wave generated in the helix after the electron has tunnelled into it from the donor molecule corresponds, in our numerical simulations, to this hybrid soliton. This hybrid soliton is not localized on a single strand, instead it is distributed between the strands and propagates along the helix with some intrinsic oscillations, rather than along a particular strand, a fact which reflects its hybrid nature. The propagation of this

localized polaron is followed by what looks like incoherent ripples. These ripples describe the radiated sound waves in the helix. This is because our system is not completely integrable and while most of the initial electron energy is transferred to the soliton, some of it is converted into oscillating soliton 'tails'.

We have then studied how  $\max|\Psi_{N+1}|^2$  varies when the acceptor parameters are varied around their optimal value. This is shown in Figs. 4-9.

To perform these simulations, we have defined the following parameters

$$D_a S = \frac{D_{a,\ell}}{J}, \quad W_a S = \frac{W_{a,\ell}}{W}, \quad X_a S = \frac{\chi_{a,\ell}}{\chi}, \quad (18)$$

which relate the different parameters of the donor and the acceptor to the corresponding ones on the peptide chain.

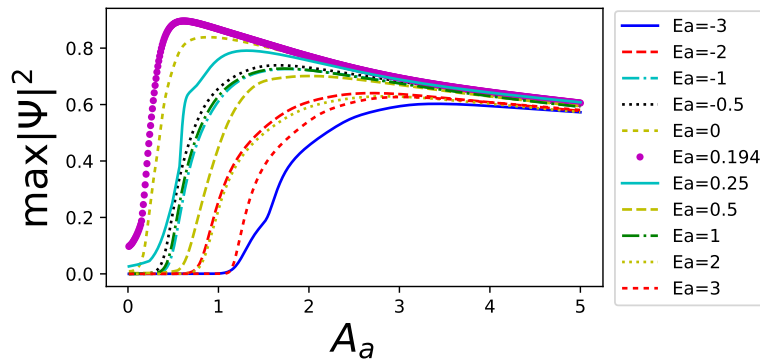


Figure 4: Full homogeneous coupling. The plot of  $\max(|\Psi_{N+1}|^2)$  for  $\tau \leq 500$  as a function of  $A_a$  for different values of  $E_a$  and the parameters values (17).

From Figs. 4 and 5, we first note that the value of the acceptor electron energy  $E_a$  has to be relatively small for the electron to be transferred to the acceptor, and that the values of  $E_a$  and  $A_a$  must be finely tuned for a good 'capture' of the electron. The parameters  $D_a$  and  $W_a$  and  $\chi_a$ , on the other hand, offer a much broader tolerance when  $E_a$  and  $A_a$  are correctly tuned (see Figs. 6 to 9). This result has a clear physical meaning, since at this last stage of the electron transport the dominant parameters are the strength of the exchange interaction of the acceptor with the helix and the value of the on-site energy level on the acceptor, while on the other hand, the electron-lattice coupling and the elasticity of the acceptor-helix bond are much less important. This being said, the last stage of the transport process is only possible if a proper soliton has been launched on the helix, carrying most of the initial energy and electron probability to the acceptor with minimal energy dissipation into the lattice vibrations and heat generation.



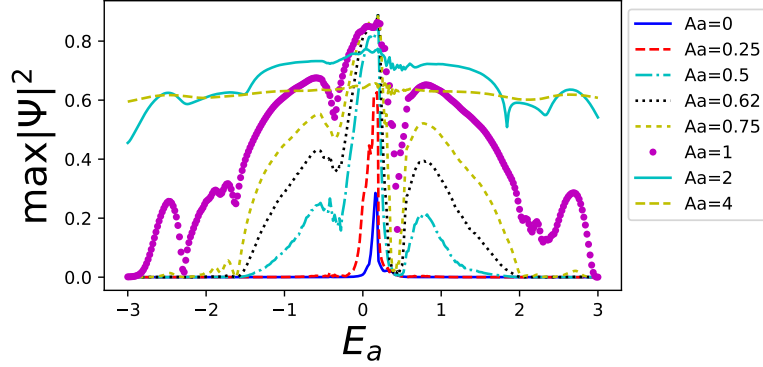


Figure 5: Full homogeneous coupling. The plot of  $\max(|\Psi_{N+1}|^2)$  for  $\tau \leq 500$  as a function of  $E_a$  for different values of  $A_{a,1} = A_{a,2} = A_{a,3} = A_a$  and the parameters values (17).

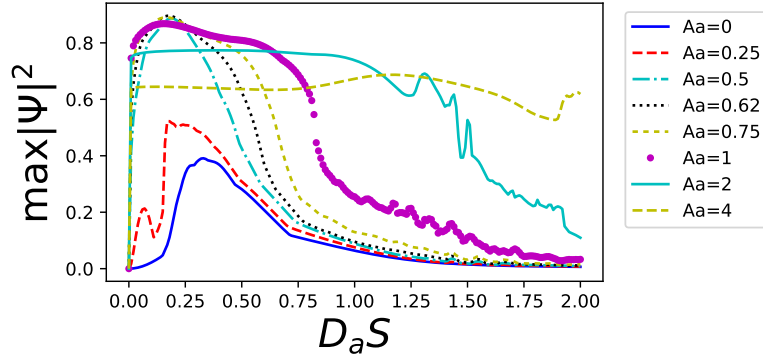


Figure 6: Full homogeneous coupling. The plot of  $\max(|\Psi_{N+1}|^2)$  for  $\tau \leq 500$  as a function of  $D_a S = D_{a,\ell}/J$  for different values of  $A_{a,1} = A_{a,2} = A_{a,3} = A_a$  and the parameters values (17).

As we will see in the next subsections, the effectiveness of the soliton formation and its parameters are determined by (i) the helix parameters, mainly by the electron-lattice coupling and strand elasticity, and (ii) by the number of helix strands coupled to the donor.

## 4.2 Single Strand Coupling

In this section we couple the donor only to the first node of the chain:  $D_{d,2} = D_{d,3} = W_{d,2} = W_{d,3} = \chi_{d,2} = \chi_{d,3} = 0$ . We obtain the best transfer from the donor to the chain for the following donor parameters:

$$E_d = 0.25, \quad D_{d,1} = 0.38 J, \quad W_{d,1} = 0.32 W, \quad \chi_{d,1} = 0.62 \chi. \quad (19)$$

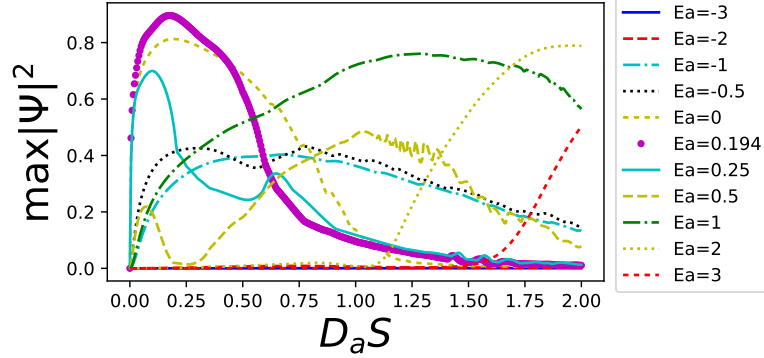


Figure 7: Full homogeneous coupling. The plot of  $\max(|\Psi_{N+1}|^2)$  for  $\tau \leq 500$  as a function of  $D_a S = D_{a,\ell}/J$  for different values of  $E_a$  and the parameters values (17).

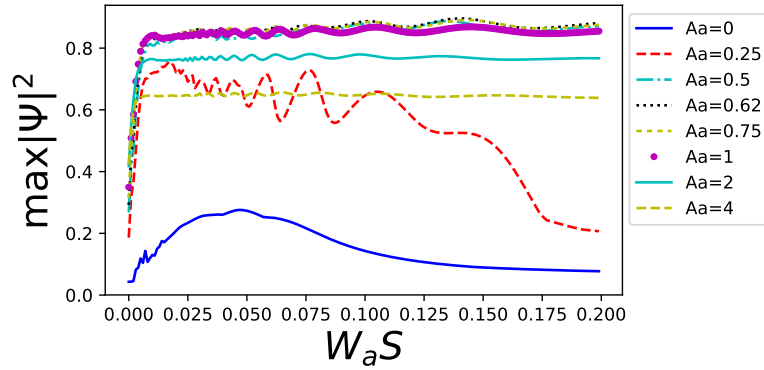


Figure 8: Full homogeneous coupling. The plot of  $\max(|\Psi_{N+1}|^2)$  for  $\tau \leq 500$  as a function of  $W_a S = W_{a,\ell}/W$  for different values of  $A_{a,1} = A_{a,2} = A_{a,3} = A_a$  and the parameters values (17).

Such conditions for creation of the soliton in the helix are not the optimal ones, since in the soliton formation there will be two contradicting tendencies: redistribution of the electron between the three peptide groups within the same unit cell and its dispersion to the nearest unit cell. These processes will be accompanied by energy dissipation much stronger than in the case of the full homogeneous coupling, and thus will result in the generation of a much weaker soliton i.e., in a less efficient transport of the electron along the helix.

Similarly, the type of coupling between the helix and the acceptor plays an important role in the electron transport, as we will see from this and the next sub-section. First, we consider the coupling of the acceptor to the same strand as the one to which the donor is coupled (single-strand coupling), setting  $A_{a,2} = A_{a,3} = D_{a,2} = D_{a,3} = W_{a,2} = W_{a,3} = \chi_{a,2} = \chi_{a,3} = 0$ .

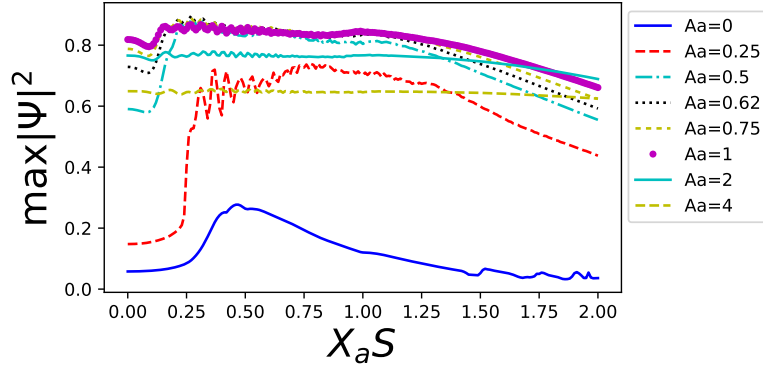


Figure 9: Full homogeneous coupling. The plot of  $\max(|\Psi|^2)$  for  $\tau \leq 500$  as a function of  $\chi_a S = \chi_{a,\ell}/\chi$  for different values of  $A_{a,1} = A_{a,2} = A_{a,3} = A_a$  and the parameters values (17).

We found that the best parameters to obtain a transfer of the electron to the acceptor are

$$\begin{aligned} E_d = 0.25, \quad D_{d,1} = 0.38 J, \quad W_{d,1} = 0.32 W, \quad \chi_{d,1} = 0.62 \chi, \quad (20) \\ A_{a,1} = 6.5, \quad E_a = 0.265, \quad D_{a,1} = 0.3 J, \quad W_{a,1} = 0.37 W, \quad \chi_{a,1} = \chi. \end{aligned}$$

As one could expect, the maximum value of the electron probability on the acceptor  $|\Psi_{N+1}|^2$  for  $\tau \leq 500$  in this case is much lower, than in the full homogeneous case, and is equal to 0.21839, only, showing that in this configuration, the electron is only transferred to acceptor with a 20% probability. As this is quite small we did not study the variation of  $\max |\Psi_{N+1}|^2$  around these optimal values of the parameters.

### 4.3 End-to-End Coupling

To couple the acceptor to the last peptide of the helix, we take  $A_{a,1} = A_{a,2} = D_{a,1} = D_{a,2} = W_{a,1} = W_{a,2} = \chi_{a,1} = \chi_{a,2} = 0$ . In this case we have obtained the best transfer using the following parameters:

$$\begin{aligned} E_d = 0.25, \quad D_{d,1} = 0.38 J, \quad W_{d,1} = 0.32 W, \quad \chi_{d,1} = 0.62 \chi, \quad (21) \\ A_{a,3} = 1.98, \quad E_a = 0.276, \quad D_{a,3} = 0.29 J, \quad W_{a,3} = 0.002 W, \quad \chi_{a,3} = 0.04 \chi, \end{aligned}$$

and, with this choice, we have found that  $\max |\Psi_{N+1}|^2 = 0.642558$ , which is higher than in the previous case, although lower than in the case of the full homogeneous coupling.

We have then studied how  $\max |\Psi_{N+1}|^2$  varies when the acceptor parameters are varied around their optimal value. This is shown in Figs. 10 to 15.

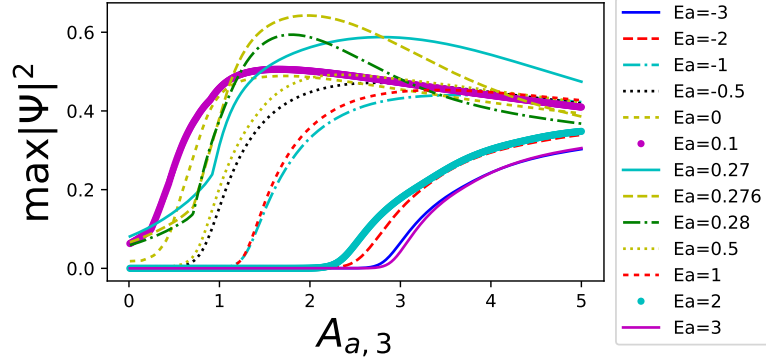


Figure 10: End-to-end coupling. The plot of  $\max |\Psi_{N+1}|^2$  for  $\tau \leq 500$  as a function of  $A_{a,3}$  for different values of  $E_a$  and the parameters values (22).

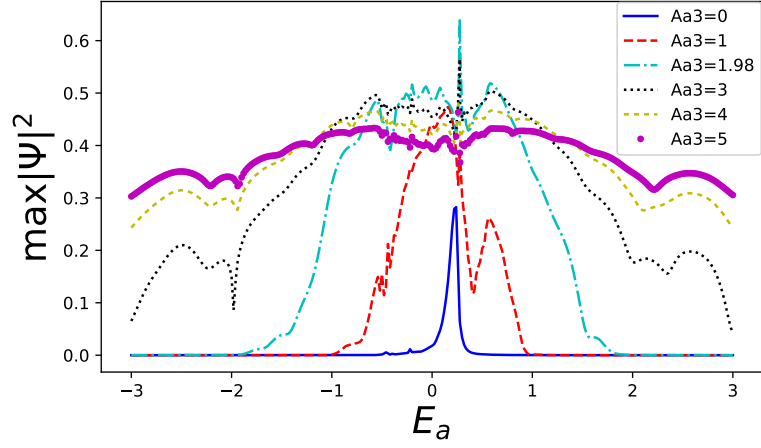


Figure 11: End-to-end coupling. The plot of  $\max |\Psi_{N+1}|^2$  for  $\tau \leq 500$  as a function of  $E_a$  for different values of  $A_{a,3}$  and the parameters values (22).

As with the full homogeneous coupling, we have found that the absorption is mainly controlled by a fine tuning between  $A_{a,3}$  and  $E_a$  but that there is a broader tolerance for the values of  $D_a$ ,  $W_a$  and  $\chi_a$ .

Having analysed the parameter stability of our model we now turn to the study of its thermal stability.

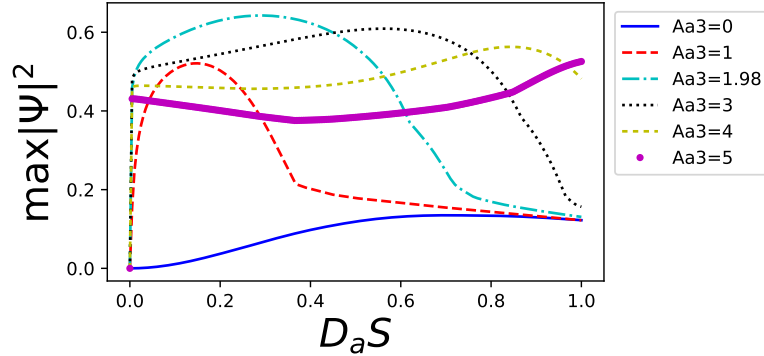


Figure 12: End-to-end coupling. The plot of  $\max |\Psi_{N+1}|^2$  for  $\tau \leq 500$  as a function of  $D_a S = D_{a,\ell}/J$  for different values of  $A_{a,3}$  and the parameters values (22).

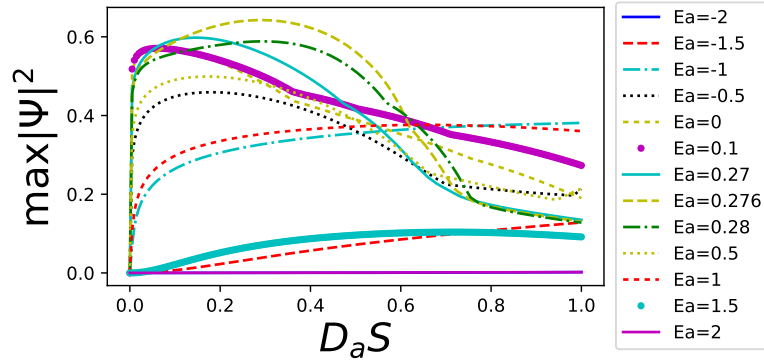


Figure 13: End-to-end coupling. The plot of  $\max |\Psi_{N+1}|^2$  for  $\tau \leq 500$  as a function of  $D_a S = D_{a,\ell}/J$  for different values of  $E_a$  and the parameters values (22).

## 5 Thermal Stability of the Soliton Mediated Electron Transport

So far, in the study of our model, we have not taken into account any thermal fluctuations. To include them we have modified the model by adding the following Langevin terms to the equations for  $U_n$ :

$$L_n = F_n(\tau) - \Gamma \frac{du_n}{d\tau}, \quad (22)$$

where  $\Gamma$  is an absorption parameter and  $F_n(\tau)$  represents the thermal noise modelled as a Gaussian white noise of zero mean value and variance given

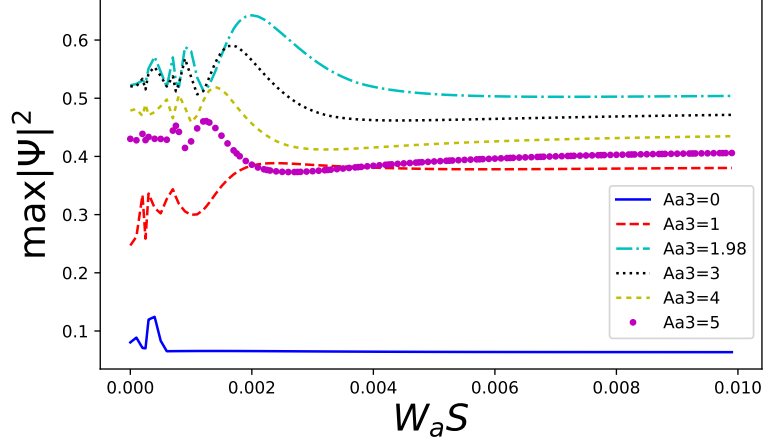


Figure 14: End-to-end coupling. The plot of  $\max |\Psi_{N+1}|^2$  for  $\tau \leq 500$  as a function of  $W_a S = W_{a,\ell}/W$  for different values of  $A_{a,3}$  and the parameters values (22).

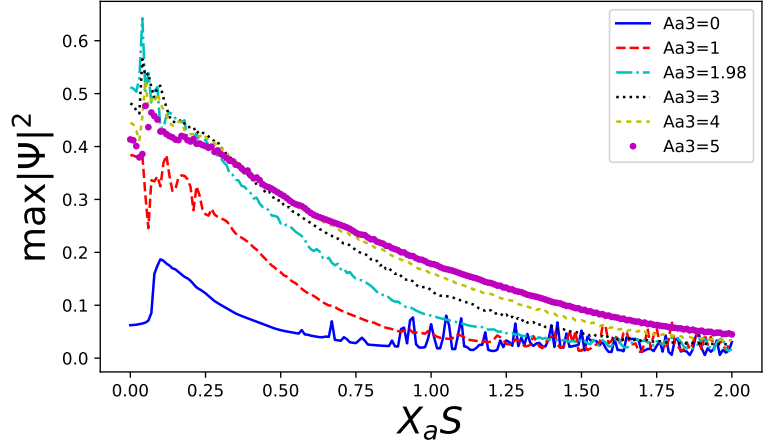


Figure 15: End-to-end coupling. The plot of  $\max |\Psi_{N+1}|^2$  for  $\tau \leq 500$  as a function of  $\chi_a S = \chi_{a,\ell}/\chi$  for different values of  $A_{a,3}$  and the parameters values (22).

by

$$\langle F_n(\tau_1) F_m(\tau_2) \rangle = 2\Gamma kT \delta(\tau_1 - \tau_2) \delta_{n,m}, \quad (23)$$

where,  $k$  is Boltzmann coefficient, and for the dimensional thermal energy  $k\bar{T}$ , we have  $kT = k\bar{T}/\hbar\nu$ . To implement this numerically,  $F(\tau)$  has to be kept constant during each time step  $d\tau$  and so we have used  $\delta(\tau_1 - \tau_2) = 1/d\tau$ .

For each temperature, we have performed 100 simulations and computed the mean values of  $\max |\Psi_a|$ , for  $\tau \leq 100$ , obtained from these simulations.

At physiological temperature,  $\overline{kT} \approx 0.025eV$  which in our adimensional units corresponds to 7.12. We have thus varied  $kT$  between 0 and 10 to capture the physiological conditions when  $\overline{J}$  is smaller than  $0.035eV$ .

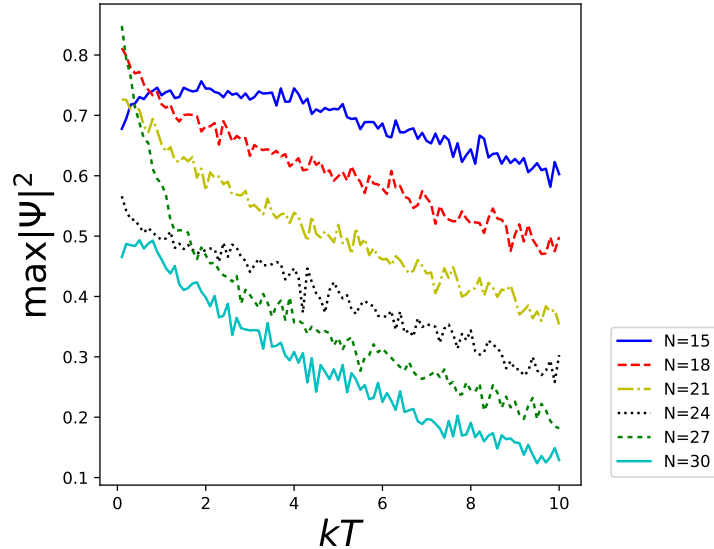


Figure 16: Full homogeneous coupling. The plot of  $\max |\Psi_{N+1}|^2$  for  $\tau \leq 100$  as a function of  $kT$  for different values of the chain length  $N$ .  $\Gamma = 0.2$ .

In Fig. 16 we present the variation of  $\max |\Psi_{N+1}|^2$  as a function of temperature for different chain lengths. We see that for short chains, the temperature has a minimal effect while for longer chains, its influence is more pronounced.

It is worth to recall that although large proteins in electron transport chains can consist of up to a few thousand aminoacids, the  $\alpha$ -helical parts of their globular structure consist of up to  $N = 50 - 70$  peptide groups. In trans-membrane proteins the  $\alpha$ -helices are even shorter, with  $N = 30$  or even smaller. Moreover, in the biggest enzymes of electron transport chain, like NADH ubiquinone oxidoreductase, which is the first and the biggest protein complex of the respiratory chain, there is a whole pathway for the electron transport prior to the ubiquinone reduction via several iron sulfur clusters, connected by relatively short  $\alpha$ -helices (see [8]). So we conclude, that under physiological conditions, the transfer of the electron from a donor to an acceptor is thermally stable.

Looking at the data in Fig. 17 we see that the probability of an electron transfer from the donor to the acceptor is relatively constant when  $\Gamma < 1$  and so that it does not play a significant role on the thermal stability of the electron transfer. In [15]  $\Gamma$ , which can only be estimated, was taken to be

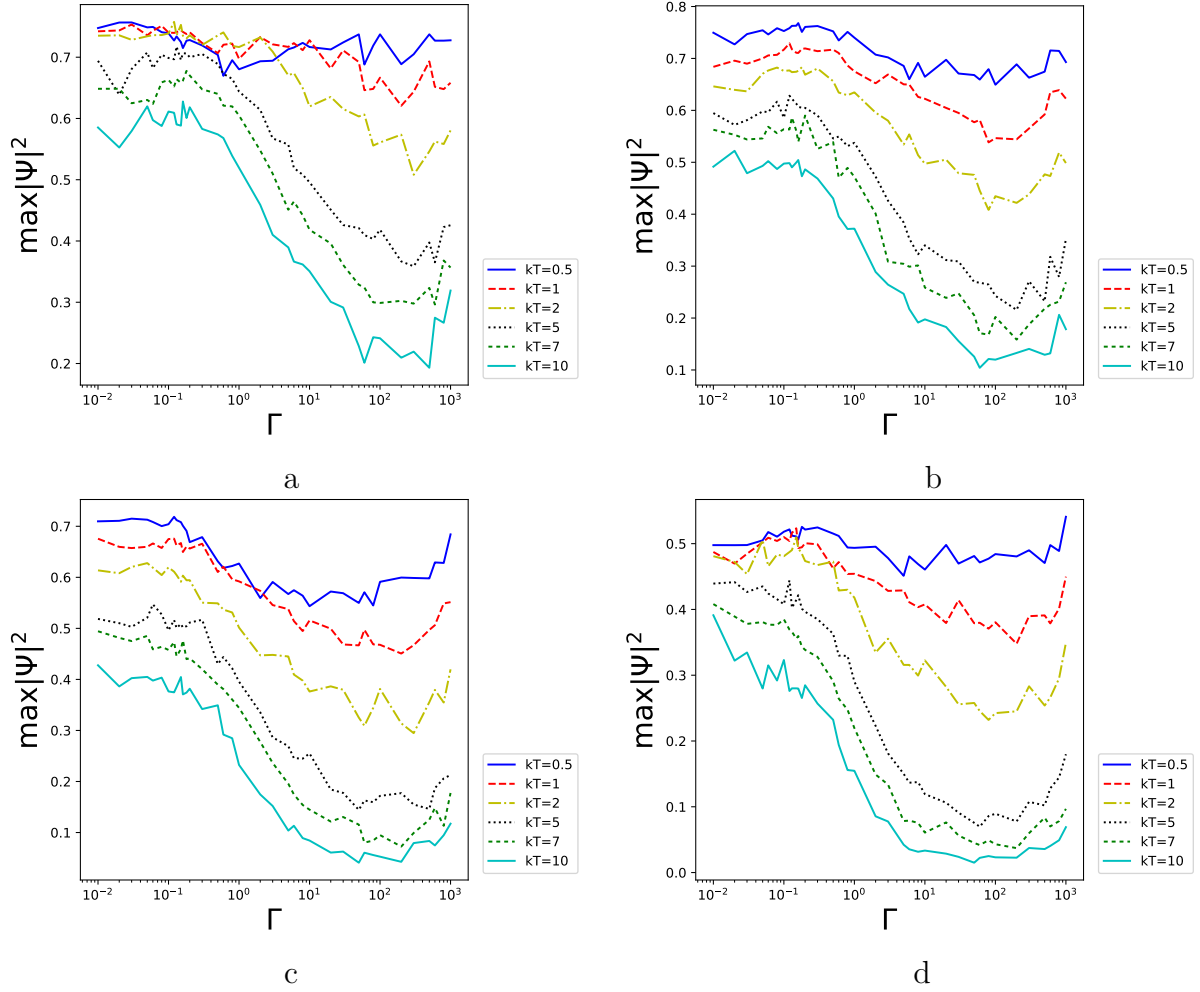


Figure 17: Full homogeneous coupling. The plot of  $\max |\Psi_{N+1}|^2$  for  $\tau \leq 500$  as a function of  $\Gamma$  for different values of  $kT$ . a)  $N = 15$ , b)  $N = 18$ , c)  $N = 21$ , d)  $N = 24$ .

0.2.

## 6 Conclusions

In this paper we have presented a model describing the long-range transport of an electron from a donor molecule to an acceptor one via the nonlinear state of a large polaron (soliton-like state) formed in a  $\alpha$ -helical protein in a ‘Donor –  $\alpha$ -helix – Acceptor’ system. Conventionally, we model the  $\alpha$ -helix as a polypeptide chain, twisted in a helix, in which each peptide



group is coupled to its nearest neighbours by a chemical bond and to every 3<sup>rd</sup> neighbour by a hydrogen bond. The helix can thus be described as 3 parallel strands coupled to each other. We have found that the static polaron on such a helix, for the parameters that describe AMID I vibration in  $\alpha$ -helical protein, is a relatively broad localized hump extended over the polypeptide macromolecule in agreement with other studies (see, e.g., [11, 13]). In our model we have only taken into account one phonon mode, while in real proteins there are many other phonon modes, the interaction with which results in bigger value of the effective electron-lattice coupling, and, hence, in stronger soliton localization than obtained here.

We have then studied the transfer of an electron from a donor molecule to the acceptor by initially placing the electron on the donor. For the proper parameters of the couplings, the electron was, within a very short time interval, transferred onto the polypeptide chain where it was self-trapped in a polaron state, and then moved towards the other extremity of the chain where it was absorbed by the acceptor.

We have considered three types of couplings between the donor and the polypeptide chain as well as between the acceptor and the polypeptide chain. In the first case, the donor and the acceptor were coupled, respectively, to the first 3 and the last 3 nodes of the chain, using the identical parameters and we called such a configuration the ‘fully homogeneous’ one. In the second configuration, the donor was coupled to the first node of the chain and the acceptor to the last node of the same strand or to the last node of the helix. We called such couplings ‘single-strand’ and ‘end-to-end’ ones, respectively.

The fully homogeneous coupling is the one that leads to the best donor-acceptor electron transport with an efficiency of 90% or more depending on the length of the chain. The ‘end-to-end’ coupling did not work so well, but still led to a transfer probability of up to 60% while the ‘single-strand’ one was the worst leading only to a 20% probability transfer. These results can be explained from the dependence of the efficiency of the soliton generation not only on the actual parameter values of the system, but also on the type of couplings between the helix and the donor and the acceptor. If one uses the inverse scattering theory for integrable system, applied to the time evolution of certain initial conditions for the nonlinear Schrödinger equation that approximates Davydov solitons [16, 17], these different couplings translate into specific initial conditions which leads to families of solitons with different efficiencies.

Our study has shown that an electron in the polaron (soliton-like) state can easily propagate as a travelling wave along the  $\alpha$ -helical chain. The polaron that is generated in the helix in the vicinity of the donor molecule has a complex internal structure: it is not just a clean simple polaron localized on

a single strand; instead, it is distributed between the strands and propagates along the helix with some intrinsic oscillations, rather than along a particular strand, which reflects its collective hybrid nature.

Unfortunately, the exact value of the exchange interaction for extra electron in proteins is not known, but can be roughly estimated at 0.05 - 0.1 eV, comparable with  $\bar{J}$ , and the other parameters are the same as for AMID I vibration, which were used in our model. Other related manufactured Donor -  $\alpha$ -helix - Acceptor systems, described in the introduction, have parameter values close to the considered here, so we can conclude that our model for the long-range electron transport describes these systems as well.

Our results explain the experimental evidence that the donor and acceptor parameters, as well as the type of their coupling affect the electron transport in 'Donor -  $\alpha$ -helix - Acceptor' systems (see [61, 62]).

We have also shown that when we add thermal fluctuations to the model, the long range electron transfer in the 'Donor -  $\alpha$ -helix - Acceptor' system is stable at physiological temperatures. We have thermalized a mixed quantum classical system in a way which makes the quantum part behave classically as well. According to [63] this results in a broadening of the soliton wave function in the helix and in a decrease of the binding energy of the soliton. This, in turn, results in a lower stability of the soliton with respect to any perturbation, including thermal fluctuations, compared to a proper analysis of the thermal stability. Moreover, as shown in [64], accounting for temperature fluctuations in the equation for lattice displacements within a quantum-mechanical description results in an effective decrease of the resonant interaction energy by the exponential Debay-Waller factor. This then leads to a decrease of the spatial dispersion of the electron and an increase of the electron-lattice coupling which itself results in an increase of the binding energy of the soliton and, as a result, a higher thermal stability compared to our model. A proper analysis of thermal stability of electron transport would require a more rigorous treatment and be the topic of a paper on its own. In this paper we have decided to restrict ourselves to the simplest analysis.

## 7 Acknowledgement

One of us, LSB, acknowledges the partial support from the budget program KPKVK 6541230 and the scientific program 0117U00236 of the Department of Physics and Astronomy of the National Academy of Sciences of Ukraine and thanks the Department of Mathematical Sciences of the University of Durham for the hospitality during her short-term visit. WJZ thanks the Leverhulme Trust for his grant EM-2016-007.

## References

- [1] J. Jortner, M. Bixon, eds *Electron Transfer From Isolated Molecules to Biomolecules*. Adv. Chem. Phys., **106**. John Wiley and Sons, Inc., New York, NY, (1999)
- [2] Voet D., Voet J.G . *Biochemistry* (3rd ed.). John Wiley and Sons. (2004). ISBN 978-0-471-58651-7.
- [3] Frster, Theodor (1948). *Annalen der Physik* (in German). 437 (12): 5575. Bibcode:1948AnP...437...55F. doi:10.1002/andp.19484370105
- [4] M. Kasha. In: M. Kasha ed., *Physical and Chemical Mechanisms in Molecular Radiation Biology*. Springer, p 231-255. (1992).
- [5] Jones, Garth A; Bradshaw, David S (2019). *Frontiers in Physics*. 7: 100.doi:10.3389/fphy.2019.00100
- [6] Murray, Robert K.; Daryl K. Granner; Peter A. Mayes; Victor W. Rodwell (2003). *Harper's Illustrated Biochemistry*. New York, NY: Lange Medical Books/ McGraw Hill. p. 96. ISBN 0-07-121766-5.
- [7] T. Althoff, D. J. Mills, J.-L. Popot, and W. Khlbrandt. *The EMBO Journal*, (2011) **30** 4652-4664.
- [8] Davydov, A.S. and Kislukha, N.I. (1973) *Physica Status Solidi* (b), **59**, 465-470. <https://doi.org/10.1002/pssb.2220590212>
- [9] A.S. Davydov, *Solitons in Molecular Systems* (Dordrecht, Reidel, (1985)).
- [10] A.C.Scott. *Phys. Rep.*, **217** 1, (1992).
- [11] A. S. Davydov, A. A. Eremko, and A. I. Sergienko, *Ukr. J. Phys.* **23**, 983, (1978)
- [12] V. K. Fedyanin and L. V. Yakushevich, *Int. J. Quantum Chem.* **21**, 1019 (1982).
- [13] L.S. Brizhik, A.A. Eremko, B. Piette W.J. Zakrzewski. *Phys. Rev. E* **70**, 031914, p.1-16, (2004).
- [14] L.S. Brizhik, A.A. Eremko, *Z. Phys. B*, **104**, 771-775, (1997).
- [15] L. Brizhik, B. Piette, W. Zakrzewski. *Phys.Rev. E* **90** 052915, (2014) DOI: <http://dx.doi.org/10.1103/PhysRevE.90.052915>

- [16] L.S. Brizhik, A.S. Davydov, Phys. Stat. Sol. (b), **115** 615-630, (1983)
- [17] L.S. Brizhik. Phys. Rev.B1, **48** 3142-3144, (1993).
- [18] D.G. Nicholls, S.J. Ferguson (2002) *Bioenergetics 3*. Academic Press. ISBN 978-0-12-518121-1.
- [19] C.W.F. McClare. Ann. N.Y. Acad. Sci. **227** 7497, (1974).
- [20] N.A. Nevskaya, Yu.N. Chirgadze. Biopolymers, **15** 639-649, (1976).
- [21] A.S. Davydov. Biology and Quantum Mechanics (Monographs in Natural Philosophy). Series: International Series in natural philosophy (Book 109) Pergamon Press; 1st edition (December 1, 1981) ISBN -13: 978-0080263922; ISBN-10: 0080263925
- [22] G. Careri. In: Cooperative Phenomenon (H.Haken and W. Wagner Eds.) Springer-Verlag, 391-394, (1973).
- [23] Ganim Z., Chung H.S., Smith A.W., Deflores L.P., Jones K.C., Tokmakoff A. Acc Chem Res. 41(3):432-41, (2008). doi: 10.1021/ar700188n. Epub 2008 Feb 21.
- [24] M.P. Marques, L.A.E. Batista de Carvalho, P.I. Harris (eds). Proceedings from the 14th European Conference on the Spectroscopy of Biological Molecules 2011, IOS Press p 316, (2013).
- [25] J.A. Roberts, J.P. Kirby, D.G. Nocera J. Am. Chem. Soc., **117** (30), pp 80518052, (1995). DOI: 10.1021/ja00135a038
- [26] Y. Zhu , R. D. Champion , S.A. Jenekhe , Macromolecules, **39** (25), 87128719, (2006); DOI: 10.1021/ma061861g
- [27] D. Li, C. Sun, H. Li, H. Shi, et al Chem. Sci., **8**, 4587-4594, (2017), DOI:10.1039/C7SC00077D
- [28] Q. Van Nguyen, P. Martin, D. Frath, et al. J. Am. Chem. Soc, 1403210131-10134, Publication Date: July 30, (2018)
- [29] L. Tian, Z. Hu, X. Liu, et al, ACS Appl. Mater. Interfaces. **11**(5) 5289-5297, (2019). doi: 10.1021/acsami.8b19036.
- [30] H. Li, F.S. Kim, G. Ren, and S.A. Jenekhe, J. Am. Chem. Soci. 135 (40), 14920-14923, (2013)

- [31] H. A. M. van Mullekom, J. A. J. M. Vekemans, E. E. Havinga, and E. W. Meijer, *Mater. Sci. Eng.* 32, 1, (2001).
- [32] Y. Zhu, R. D. Champion, and S. A. Jenekhe, *Macromolecules*, 39, 8712, (2006).
- [33] G. Yu, J. Gao, J. C. Hummelen, F. Wudl, and A. J. Heeger, *Science* 270, 1789, (1995).
- [34] L.M. Campos, A. Tontcheva, S. Günes, G. Sonmez, Neugebauer, N. S. Sariciftci, and F. Wudl, *Chem. Mater.* 17, 4031, (2005).
- [35] M. Svensson, F. Zhang, S. C. Veenstra, W. J. H. Verhees, C. Hummelen, J. M. Kroon, O. Inganäs, and M. R. Andersson, *Adv. Mater.* 15, 988, (2003).
- [36] S. Admassie, O. Inganäs, W. Mammo, E. Perzon, and M. R. Andersson, *Synth. Met.* 156, 614 (2006).
- [37] A. P. Kulkarni, Y. Zhu, and S. A. Jenekhe, *Macromolecules* 38, 1553, (2005).
- [38] C. Ego, D. Marsitzky, S. Becker, J. Zhang, A. C. Grimsdale, Mullen, J. D. MacKenzie, C. Silva, and R. H. Friend, *J. Am. Chem. Soc.* 125, 437, (2003)
- [39] Thompson, B. C., Madrigal L. G., Pinto M. R., Kang T.-S., Schanze K. S., Reynolds J. R., *J. Polym. Sci., Part A: Polym. Chem.* 43, 1417, (2005).
- [40] Wu W.-C., Liu, C.-L., Chen, W.-C., *Polymer*, 47, 527, (2006).
- [41] Babel, J. D. Wind, and S. A. Jenekhe, *Adv. Funct. Mater.* 14, 891, (2004).
- [42] T. Yamamoto, T. Yasuda, Y. Sakai, and S. Aramaki, *Macromol. Rapid Commun.* 26, 1214, (2005).
- [43] T. Yasuda, Y. Sakai, S. Aramaki, and T. Yamamoto, *Chem. Mater.* 17, 6060, (2005)
- [44] Sh. Chen, K. C. Lee, Z.-G. Zhang, et al., *Macromolecules* 49 527-536, (2016). DOI: 10.1021/acs.macromol.5b02324
- [45] H. Zhang, S. Zhang, Y. Mao, et al. *Polym. Chem.*, 8, 3255-3260, (2017), DOI:10.1039/C7PY00616K

- [46] M. Chen, X. Crispin, E. Perzon, M. R. Andersson, T. Pullerits, M. Andersson, O. Inganäs, and M. Berggren, *Appl. Phys. Lett.* **87**, 252105, (2005).
- [47] L. Sepunaru, S. Refaely-Abramson, R. Lovrincic, et al., *Structure*, *J. Am. Chem. Soc.*, **137** 30 9617-9626, (2015).
- [48] P. G. M. Mileo, K. Adil, L. Davis, et al., *J. Am. Chem. Soc.* **140** 13156-13160, (2018)
- [49] N. L. Ing, M.Y. El-Naggar, A.I. Hochbaum. *J. Phys. Chem. B* **122** 10403-10423, (2018)
- [50] N. Amdursky. Enhanced Solid-State Electron Transport via Tryptophan Containing Peptide Networks. *Phys. Chem. Chem. Phys.* , **15** 13479-13482, (2013)
- [51] S. Xu, A. Barrozo, L.M. Tender, et al., Cytochrome Mediated Redox Conduction through *Shewanella Oneidensis* MR-1 Cells. *J. Am. Chem. Soc.* **140** 10085-10089, (2018)
- [52] S. K. M. Nalluri, C. Berdugo, N. Javid, et al., Biocatalytic Self-Assembly of Supramolecular Charge Transfer Nanostructures Based on n-Type Semiconductor-Appended Peptides. *Angew. Chem., Int. Ed.* , **53** 5882-5887, (2014).
- [53] Y. Tan, R.Y. Adhikari, N.S. Malvankar, et al., Synthetic Biological Protein Nanowires with High Conductivity. *Small* **12** (33), 4481-4485, (2016). doi.org/10.1002/sml.201601112
- [54] B. Akdim, R. Pachter, R.R. Naik. Self-Assembled Peptide Nanotubes as Electronic Materials: An Evaluation from FirstPrinciples Calculations. *Appl. Phys. Lett.* **106** (18), 183707, (2015).
- [55] A.S. Davydov and A.D. Suprun. *Ukr. J. Phys.* **19** 44, (1974).
- [56] G.S. Engel, T.R. Calhoun, E.L. Read, T.K. Ahn, T. Mancal, Y.C. Cheng, R.E. Blankenship and G.R. Fleming. *Nature* **446** 782786, (2007).
- [57] E. Collini, C.Y. Wong, K.E. Wilk, P.M.G. Curmi, P. Brumer and G.D. Scholes. *Nature* **463** 644647, (2010)
- [58] T. Renger, V. May, O. Kühn, *Phys. Rep.* **343** 137, (2001).

- [59] H. Wang, S. Lin, J.P. Allen, J.C. Williams, S. Blankert, C. Laser, N.W. Woodbury, *Science* **316** 747, (2007).
- [60] Donald J. Voet; Judith G. Voet; Charlotte W. Pratt (2008). "Chapter 18, Mitochondrial ATP synthesis". *Principles of Biochemistry*, 3rd Edition. Wiley. p. 608. ISBN 978-0-470-23396-2
- [61] X. U. Jiang, K. Ataka, and J. Heberle. Influence of the molecular structure of carboxyl-terminated self-assembled monolayer on the electron transfer of cytochrome c adsorbed on an electrode: In situ observation by surface-enhanced infrared absorption spectroscopy. *J. Phys. Chem. C* **112** 813-819, (2008).
- [62] H. Guo, T. Kimura, and Y. Furutani. Distortion of the amide-I and -II bands of an  $\alpha$ -helical membrane protein, pharaonis halorhodopsin, depends on thickness of gold films utilized for surface-enhanced infrared absorption spectroscopy. *Chem. Phys.* **419** 8-16, (2013)
- [63] L. Cruzeiro-Hansson. *Phys. Rev. E* , **56** 894, (1997)
- [64] L.S. Brizhik, A.S. Davydov, I.M. Pershko, *Theor. Math. Fiz.*, 77, 179-189, (1988)